Article:
Gala de Pablo, J., Lindley, M., Hiramatsu, K. et al. (1 more author) (2021) High-Throughput Raman Flow Cytometry and Beyond. Accounts of Chemical Research, 54 (9). pp. 2132-2143. ISSN 0001-4842

https://doi.org/10.1021/acs.accounts.1c00001

High-throughput Raman flow cytometry and beyond

Julia Gala de Pablo[1], Matthew Lindley[1], Kotaro Hiramatsu[1,2,3,4], and Keisuke Goda[1,5,6]*

[1] Department of Chemistry, The University of Tokyo, 7-3-1 Hongo, Bunkyo-ku, Tokyo 113-8654, Japan

[2] Kanagawa Institute of Industrial Science and Technology, 705-1 Shimoimaizumi, Ebina, Kanagawa 243-0435, Japan

[3] Research Center for Spectrochemistry, The University of Tokyo, 7-3-1 Hongo, Bunkyo-ku, Tokyo 113-0033, Japan

[4] PRESTO, Japan Science and Technology Agency, 4-1-8 Honcho, Kawaguchi, Saitama 332-0012, Japan.

[5] Department of Bioengineering, University of California, 410 Westwood Plaza, Los Angeles CA 90095, California, United States

[6] Institute of Technological Sciences, Wuhan University, Wuchang District, Wuhan 430072, Hubei, China

CONSPECTUS

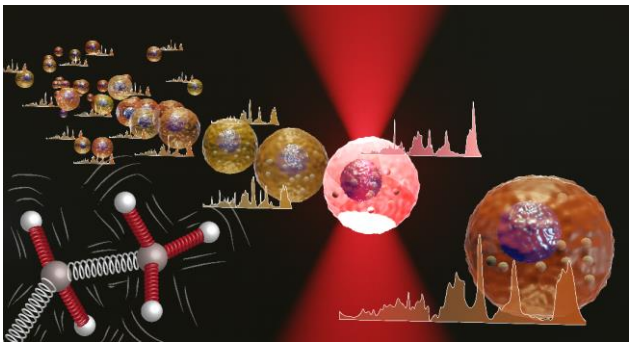

Flow cytometry is a powerful tool with applications in diverse fields such as microbiology, immunology, virology, cancer biology, stem cell biology, and metabolic engineering. It rapidly counts and characterizes large heterogeneous populations of cells in suspension (e.g., blood cells, stem cells, cancer cells, microorganisms) and dissociated solid tissues (e.g., lymph nodes, spleen, solid tumors) with typical throughputs of 1,000 - 100,000 events per second (eps). By measuring cell size, cell granularity, and the expression of cell surface and intracellular molecules, it provides systematic insights into biological processes. Flow cytometers may also include cell sorting capabilities to enable subsequent additional analysis of the sorted sample (e.g., electron microscopy, DNA/RNA sequencing), cloning, and directed evolution. Unfortunately, traditional flow cytometry has several critical limitations as it mainly relies on fluorescent labeling for cellular phenotyping, which is an indirect measure of intracellular molecules and surface antigens. Furthermore, it often requires time-consuming preparation protocols and is incompatible with cell therapy. To overcome these difficulties, a different type of flow cytometry based on direct measurements of intracellular molecules by Raman spectroscopy, or "Raman flow cytometry" for short, has emerged. Raman flow cytometry obtains a chemical fingerprint of the cell in a non-destructive manner, allowing for single-cell metabolic phenotyping. However, its slow signal acquisition due to the weak light-molecule interaction of spontaneous Raman scattering prevents the throughput necessary to interrogate large cell populations in reasonable time frames, resulting in throughputs of about 1 eps. The remedy to this throughput limit lies in coherent Raman scattering methods such as stimulated Raman scattering (SRS) and coherent anti-Stokes Raman scattering (CARS), which offer a significantly enhanced light-sample interaction and hence enable high-throughput Raman flow cytometry, Raman imaging flow cytometry, and even Raman image-activated cell sorting (RIACS). In this Account, we outline recent advances, technical challenges, and emerging opportunities of coherent Raman flow cytometry. First, we review the principles of various types of SRS and CARS and introduce several techniques of coherent Raman flow cytometry such as CARS, multiplex CARS, Fourier-transform CARS, SRS, SRS imaging flow cytometry, and RIACS. Next, we discuss a unique set of applications enabled by coherent Raman flow cytometry, from microbiology and lipid biology to cancer detection and cell therapy. Finally, we describe future opportunities and challenges of coherent Raman flow cytometry including increasing sensitivity and throughput, integration with droplet microfluidics, utilizing machine learning techniques, or achieving in vivo

flow cytometry. This Account summarizes the growing field of high-throughput Raman flow cytometry and the bright future it can bring.

KEY REFERENCES

- Hiramatsu, K.; Ideguchi, T.; Yonamine, Y.; Lee, S.; Luo, Y.; Hashimoto, K.; Ito, T.; Hase, M.; Park, J.-W.; Kasai, Y.; Sakuma, S.; Hayakawa, T.; Arai, F.; Hoshino, Y.; Goda, K. High-Throughput Label-Free Molecular Fingerprinting Flow Cytometry. *Science Advances* **2019**, *5* (1), eaau0241.[1] *This work reports fingerprint-region coherent Raman flow cytometry based on Fourier-transform coherent anti-Stokes Raman scattering with a record throughput of ~1,000 eps.*
- Hiramatsu, K.; Yamada, K.; Lindley, M.; Suzuki, K.; Goda, K. Large-Scale Label-Free Single-Cell Analysis of Paramylon in Euglena Gracilis by High-Throughput Broadband Raman Flow Cytometry. *Biomedical Optics Express* **2020**, *11* (4), 1752.[2] *This work demonstrates single-cell analysis of Euglena gracilis using Fourier-transform coherent anti-Stokes Raman scattering with a throughput >1,000 cells/s*
- Suzuki, Y.; Kobayashi, K.; Wakisaka, Y.; Deng, D.; Tanaka, S.; Huang, C.-J.; Lei, C.; Sun, C.-W.; Liu, H.; Fujiwaki, Y.; Lee, S.; Isozaki, A.; Kasai, Y.; Hayakawa, T.; Sakuma, S.; Arai, F.; Koizumi, K.; Tezuka, H.; Inaba, M.; Hiraki, K.; Ito, T.; Hase, M.; Matsusaka, S.; Shiba, K.; Suga, K.; Nishikawa, M.; Jona, M.; Yatomi, Y.; Yalikun, Y.; Tanaka, Y.; Sugimura, T.; Nitta, N.; Goda, K.; Ozeki, Y. Label-Free Chemical Imaging Flow Cytometry by High-Speed Multicolor Stimulated Raman Scattering. *PNAS* **2019**, *116* (32), 15842–15848. [3] *This work reports coherent Raman imaging flow cytometry in the high-frequency region based on stimulated Raman scattering with a record throughput of ~100 eps.*
- Nitta, N.; Iino, T.; Isozaki, A.; Yamagishi, M.; Kitahama, Y.; Sakuma, S.; Suzuki, Y.; Tezuka, H.; Oikawa, M.; Arai, F.; Asai, T.; Deng, D.; Fukuzawa, H.; Hase, M.; Hasunuma, T.; Hayakawa, T.; Hiraki, K.; Hiramatsu, K.; Hoshino, Y.; Inaba, M.; Inoue, Y.; Ito, T.; Kajikawa, M.; Karakawa, H.; Kasai, Y.; Kato, Y.; Kobayashi, H.; Lei, C.; Matsusaka, S.; Mikami, H.; Nakagawa, A.; Numata, K.; Ota, T.; Sekiya, T.; Shiba, K.; Shirasaki, Y.; Suzuki, N.; Tanaka, S.; Ueno, S.; Watarai, H.; Yamano, T.; Yazawa, M.; Yonamine, Y.; Di Carlo, D.; Hosokawa, Y.; Uemura, S.; Sugimura, T.; Ozeki, Y.; Goda, K. Raman Image-Activated Cell Sorting. *Nature Communications* **2020**, *11* (1), 3452.[4] *This is the first report of Raman image-activated cell sorting that achieves a high throughput of ~100 eps.*

1. INTRODUCTION

Flow cytometry is a powerful tool that has numerous applications in diverse fields such as microbiology, immunology, virology, cancer biology, stem cell biology, and metabolic engineering[5–9]. It rapidly counts and characterizes large heterogeneous populations of cells in suspension (e.g., blood cells, stem cells, microorganisms) by measuring cell size, cell granularity, and the expression of cell surface and intracellular molecules with throughputs of 1,000 - 100,000 events per second (eps) – where an event is defined as a single cell, a cell cluster, or a piece of cell debris detected by the system –, providing systematic insights into biological processes[10]. It also handles solid tissues (e.g., lymph nodes, spleen, mucosal tissues, solid tumors) that can be dissociated into single cells[11]. In addition to the analysis of cell populations, the ability to sort target cells from mixed populations is essential for further analysis (e.g., electron microscopy, DNA/RNA sequencing), cloning, and directed evolution, as represented by fluorescence-activated cell sorting (FACS)[12]. Traditionally, the instrumentation of typical flow cytometers involves fluidics, optics, electronics, and data analysis[13]. Specifically, multiple lasers are used to interrogate a single stream of flowing cells focused passively or actively in a capillary tube or microfluidic channel, followed by the measurement of fluorescence signals from the cells by sensitive photodetectors and the statistical analysis of the detected events in a multi-parametric histogram or scatter plot[14].

Unfortunately, traditional flow cytometry has several critical limitations as it mainly relies on fluorescent labeling for cellular phenotyping, an indirect measure of intracellular molecules and surface antigens (Table 1). First, fluorescent probes are typically bulky and often perturb the function of small biomolecules such as metabolites[15]. Second, fluorescent labeling is not applicable to all types of cells (e.g., bacteria, microalgae) due to the unavailability or unstable binding efficiency of fluorescent probes or due to interfering autofluorescence[16]. Third, immunofluorescent staining is remarkably difficult for labeling intracellular molecules in live cells due to the low permeability of cellular membranes and also requires accounting for unwanted side effects such as non-specific binding[17]. Fourth, while fluorescent fusion proteins allow for highly specific labeling of intracellular proteins, gene transfection is required, but not available for all cell types and proteins[18]. Fifth, without the molecular specificity provided by these labeling methods, intracellular fluorescent staining with fluorescent dyes suffers from non-specific binding and low quantitative performance since it depends on the difference in their chemical affinity to target biomolecules[19]. Sixth, the process of fluorescent labeling can be laborious, costly, and time-consuming and may affect the results of time-sensitive samples[20]. Lastly, fluorescent labeling can introduce xenobiotic compounds and lead to immunogenicity, such that human cells including human induced pluripotent stem cells (hiPSCs) and chimeric antigen receptor T (CAR-T) cells cannot be fluorescently labeled before their injection to the human body for cell therapies[21,22].

To overcome these limitations, a different type of flow cytometry based on direct measurements of intracellular molecules by Raman spectroscopy, or "Raman flow cytometry" for short, has emerged[23] (Table 1). The principle of Raman spectroscopy is the inelastic scattering of incident photons by molecular vibrations so that it can be used to probe single live cells via intracellular molecular vibrations without the need for fluorescent labeling. Since Raman flow cytometry directly interrogates intracellular molecules in a label-free manner, it is free from the aforementioned limitations associated with fluorescent labeling. Moreover, the narrow spectral features of Raman flow cytometry offer much richer cellular information than traditional flow cytometry which only provides up to several colors (contrasting fluorophores) due to their spectral overlap[24]. While Raman flow cytometry holds the promise of large-scale label-free cell analysis, the slow signal acquisition of Raman spectroscopy due to the weak light-molecule interaction of spontaneous Raman scattering (RS) results in typical throughputs below 1 eps (Figure 1a), preventing the interrogation of large cell populations[24].

The remedy to this throughput limit lies in coherent Raman scattering (CRS) methods[24], which significantly enhance light-sample interaction and allow higher throughput than spontaneous RS (Table 1, Figures 1b-1d). CRS methods utilize strong laser pulses, called "pump" and "Stokes", to create a phase coherence in molecular vibrations along the optical path. The Raman-scattered light from these coherently driven molecules adds up constructively, producing several orders of magnitude stronger signals than spontaneous RS measurements[25]. The higher signal level of CRS is employed to reduce the spectral acquisition time from ~1 s orders of spontaneous Raman to ~1 ms and even ~1 μs orders, facilitating applications such as video-rate Raman imaging[26] and high-throughput Raman flow cytometry. Specifically, two approaches to CRS dominate the current practice: stimulated Raman scattering (SRS)[27] (Figure 1b) and coherent anti-Stokes Raman scattering (CARS)[25] (Figure 1c). In fact, several papers about the experimental demonstration of high-throughput Raman flow cytometry based on SRS and CARS have been reported[1–4,28–31].

In this Account, we outline recent advances, technical challenges, and emerging opportunities of coherent Raman flow cytometry for high-throughput analysis. First, we review the principles of various types of SRS and CARS and introduce several techniques of coherent Raman flow cytometry. Next, we discuss a unique set of applications enabled by coherent Raman flow cytometry. Finally, we describe future opportunities and challenges of coherent Raman flow cytometry.

2. COHERENT RAMAN SCATTERING FOR RAMAN FLOW CYTOMETRY

In CRS, incident photons can scatter to lower frequencies (Stokes scattering) or to higher frequencies (anti-Stokes scattering). The magnitude of this frequency shift identifies molecular vibrational energy levels in the sample and is reported as a spectrum in units of cm^{-1}. The two most relevant regions of the spectrum for cell analysis are the "fingerprint" region (500-1800 cm^{-1}) and the "high-wavenumber" region (2800-3800 cm^{-1}), with a spectral "silent" region (1800-2800 cm^{-1}) in between[32]. Raman spectra identify small molecules with high specificity, but lose specificity among large biomolecules with repeated functional groups, such as proteins and nucleic acids. The silent region, empty of Raman signals from biomolecules, is excellent for labelling schemes using probes containing deuterium bonds and alkynes[33].

Since the first demonstration of SRS in 1962[34] and CARS in 1965[35], both methods have been optimized to a wide range of applications. For Raman flow cytometry this optimization consists of balancing trade-offs between resolution, bandwidth, and throughput: molecular information grows with increases in resolution and bandwidth while throughput decreases. Current SRS and CARS spectrometers typically use pulsed lasers to interact with the sample, with pulse widths in the ps or fs range (Figures 1b-1d). Short pulses have a high photon intensity, necessary to drive CRS processes, while minimizing laser-induced thermal damage[36]. Additionally, the spectral width of a laser is inversely related to its pulse width, such that a short pulse width enables single-pulse broadband measurement. This eliminates the need to scan the laser frequency, which is typically too slow for high-throughput measurement. As an additional consideration, CRS methods require a tight beam focus to produce a signal, resulting in a small acquisition volume at the beam focus relative to cell size. While this brings high intracellular spatial resolution, it also necessitates spatial beam scanning for imaging or whole-cell measurement. A brief description of CRS methods follows, with a focus on work relevant to high-throughput Raman flow cytometry.

2.1. Stimulated Raman scattering (SRS)

In SRS, pump and Stokes photons from separate laser sources are combined to drive vibrational excitation in the sample[37]. This stimulated process annihilates a pump photon and creates a second Stokes photon when the difference in photon energy matches a vibrational transition energy in the sample (Figure 1b). Molecular vibrations are detected as a loss in photon count (stimulated Raman loss; SRL) in the pump beam or as a gain in photon count (stimulated Raman gain; SRG) in the Stokes beam. These signals are quite small and can be overwhelmed by detector noise, such that one beam is modulated in time and lock-in-amplification is employed to facilitate detection. Generally, SRS spectra are produced by scanning the optical frequency between pump and Stokes lasers. Alternatively, using a broadband laser to provide one beam can cover the desired spectral range in a single pulse, eliminating the need of scanning the laser. Broadband SRS produces a spectrum every 5 - 300 μs[31,38]. Even shorter acquisition times can be realized with careful management of the trade-off between bandwidth and temporal resolution. For example, Wakisaka *et al*. demonstrated SRS using a synchronized pair of pulsed lasers, where pump pulses were entrained with wavelength-switchable Stokes pulses, achieving high-contrast four-color SRS of cellular biomolecules at an acquisition time of just ~630 ns[39] per spectrum.

2.2. Coherent anti-Stokes Raman scattering (CARS)

In CARS, pump and Stokes pulses first drive a vibrational coherence within the sample. This vibrational coherence is then interrogated by a probe pulse, with probe photons scattering inelastically off the driven vibrations to receive an anti-Stokes (blue) shift (Figure 1c). The magnitude of this shift corresponds to the energy of the vibrational transition and has the benefit of spectrally separating the signal light from the laser-driven fluorescence emission of the sample, which is generally red-shifted. Several CARS techniques have been implemented for high-throughput biological measurement, with some achieving broadband spectra at a sub-ms

repetition rate[40,41]. However, a persistent challenge in these frequency-domain CARS techniques is their susceptibility to non-resonant background (NRB). The intense laser pulses used to drive the CARS process also induce non-resonant light-matter interactions within the sample, which provide a strong spectral background of anti-Stokes-shifted probe light. Significant efforts have gone towards experimental designs and analysis techniques that remove this distortion[42–44]. Alternatively, as NRB has a short lifetime (~fs) in comparison with the coherence lifetime (~ps) of molecular vibrations[45], it can be largely avoided by delaying the arrival of the probe pulse until pump-driven NRB has subsided[46]. This is neatly accomplished by Fourier-transform CARS (FT-CARS)[47], which employs an interferometric pump-probe measurement scheme where probe light is delayed to interact with the sample after the pump-driven NRB decay (Figure 1d). By combining the FT-CARS scheme with a lab-built ultrafast interferometer, NRB-free and fingerprint-region-spanning Raman spectra can be produced within 42 μs[48,49].

2.3. Comparison between SRS and CARS

Although the information provided by SRS and CARS is identical in principle, these methods are used differently, depending on the application. A notable advantage of SRS is the absence of the non-resonant background, which makes the measured signal proportional to the concentration of the molecules. On the other hand, detection of SRS signals requires a highly stable pulse source in combination with a lock-in amplifier or tuned amplifier (TAMP). This makes broadband SRS measurement, especially in the fingerprint region, more technically challenging than broadband CARS measurement because the use of stable broadband light sources and multi-channel lock-in amplifiers or a TAMP array necessitates the development of a highly customized system with non-commercially available components.

3. TECHNIQUES OF COHERENT RAMAN FLOW CYTOMETRY

Common among all coherent Raman flow cytometry techniques is the need to flow cells through the optical interrogation region at high rates. This is generally achieved using microfluidics, where a sample of suspended cells is pumped through a microcapillary or microchannel in a glass or polymer device, with channel cross-sections typically of tens-to-hundreds of micrometers. To increase throughput and measurement reproducibility, the cells may be focused by hydrodynamic or acoustic forces so that they flow singly and at constant velocity through the optical interrogation region[50]. Following the interrogation, the cells flow through an on-chip outlet. To meet needs such as rare-cell isolation and cell-line purification, setups incorporate on-chip sorting technology, where cells are sorted in real time to collection and waste channels according to features in their Raman spectra[4,24]. Here we review the technical characteristics of the coherent Raman flow cytometry techniques reported in the literature to date.

3.1. CARS flow cytometry

CARS flow cytometry was first demonstrated by Wang *et al*. in 2008[28], by coupling a CARS microscope with a polydimethylsiloxane (PDMS) microfluidic channel and syringe pumps (Figure 2a). PDMS, often a challenge for spontaneous Raman applications due to its strong background, had no CARS background, thanks to the high confocality of CRS processes. The microfluidic device consisted of a 200 μm x 60 μm channel with hydrodynamic cell focusing. The optical system incorporated two temporally overlapped 5 ps pulse lasers. The center frequencies of the lasers were offset to provide a spectral difference of ~2840 cm^{-1} between pump and Stokes pulses necessary for the measurement of CH-stretching in the high-wavenumber region. Photomultiplier tubes detected the CARS signal in both the forwards- and backwards-scattering directions. Cell measurement was performed at a single spectral point in the CH-stretching region. Spatially scanning the laser focal spot

perpendicular to the flow direction produced CARS intensity images and sizing the cells under flow. Wang *et al.* calculated a maximum potential throughput of 100 eps in their setup for distortion-free CARS imaging[28].

3.2. Multiplex CARS flow cytometry

CARS flow cytometry progressed from single-frequency to broadband spectral measurement with the work of Camp *et al*. in 2011 (Figure 2b)[30]. In this work, they developed a technique called multiplex CARS (MCARS), which utilized a broadband coherent light source to provide Stokes photons. This setup was capable of exciting all Raman modes from 1200 to 3100 cm^{-1}, ranging from the upper fingerprint and silent to the lower high-wavenumber regions, with each CARS pulse, negating the need for frequency scanning and enabling broadband, high-throughput measurement. The incorporated microfluidic chip was commercially purchased and utilized sheath flow for hydrodynamic cell focusing. As a proof-of-concept demonstration, they measured yeast cells in flow at a throughput of up to 100 eps, limited by detector design. Based on the sensitivity of their flow cytometer, Camp *et al*. extrapolated a throughput of up to 10,000 eps to be possible following modifications to the detector[30].

3.3. FT-CARS flow cytometry

In 2019, Hiramatsu *et al*. demonstrated the first high-throughput Raman flow cytometry spanning the fingerprint region (Figure 2c)[1]. This work utilized a mode-locked 750-950 nm femtosecond pulse laser coupled with a rapid-scan Michelson interferometer to produce NRB-free FT-CARS spectra spanning 400 - 1600 cm^{-1} with a spectral resolution of 20 cm^{-1}. The microfluidic chip consisted of a 300 µm x 200 µm (width x height) main channel, etched from a silicon layer sandwiched between glass layers[51]. Acoustic focusing of the cells was achieved using a piezoelectric transducer attached to the microfluidic chip and driven with a ~3.6 MHz sine wave. This created a two-dimensional standing wave parallel to the channel cross-section throughout the channel volume. As cells flowed, they focused at the standing-wave node at the channel center. The authors demonstrated throughputs of up to ~1500 eps with a static beam focus. Importantly, the high spectral resolution of the flow cytometer allowed isotope-sensitive measurement, with stable isotope carbon substitution used to track longitudinal metabolic dynamics[1].

3.4. SRS flow cytometry

SRS flow cytometry was first demonstrated by Zhang *et al.* in 2017 (Figure 2d)[31]. Their setup consisted of an SRS spectrometer that utilized broadband pump and narrowband Stokes pulses. The spectrometer measured SRL in the pump beam with a 32-photodiode pixel array with a spectral acquisition time of 5 µs. This allowed broadband SRS measurement of 32 spectral points across its 200 cm^{-1} bandwidth with a spectral resolution of 20 cm^{-1}, making it ideal for measuring CH-stretch in the high-wavenumber region. The flow channel consisted of a capillary tube with an inner diameter of 70 µm with no cell focusing. They demonstrated a throughput of ~540 eps although they estimated only 16% of the flowed cells passed through the measurement region.[31]

3.5. SRS imaging flow cytometry

Although technically more challenging, imaging flow cytometry has the advantage of adding morphological information to the molecular-vibrational information. SRS imaging flow cytometry was first demonstrated by Suzuki *et al.* in 2019 (Figure 3e)[3]. This setup used fast-wavelength switching optics to rapidly cycle Stokes pulses between four colors, allowing the SRS imaging flow cytometer to measure four spectral points across the high-wavenumber region from 2800 to 3100 cm^{-1} at a high rate of 210 ns per spectrum. The glass-silicon-glass microfluidic device consisted of a 200 µm square channel with acoustic cell focusing. Two-dimensional imaging was accomplished by rapid resonant galvanometric beam scanning in the direction perpendicular to the flow,

allowing metabolic imaging of the cells. Maximum throughputs ranged between ~35 eps for microalgae and 140 eps for human cells[3].

3.6. SRS image-activated cell sorting

The first demonstration of Raman image-activated cell sorting was reported by Nitta *et al.* in 2020 (Figure 3e)[4]. Directly expanding on the 2019 work of Suzuki *et al.*, Nitta *et al.* implemented sorting microfluidics controlled by real-time intelligent image analysis into the earlier SRS imaging flow cytometer. The sorting chip accommodated two reservoirs located after the measurement region and connected to both sides of the flow channel. Piezoelectric actuators mounted atop the reservoirs operated in a push-pull configuration to squirt a jet of flow media across the channel, pushing or pulling target cells into side channels connected to the sorting outlet, with the center channel connected to waste[51]. Modification to the optics and detector were also made, with galvanometric beam scanning discarded in favor of a line-focus beam profile (24 µm x 1 µm, orthogonal to the flow) through which the cells passed. Detection was accomplished with a 24-pixel photodiode array. This change in detection scheme helped minimize image reconstruction time compared to the previous SRS imaging flow cytometer, a necessity for high-throughput sorting based on image analysis. Both real-time image analysis and sort control were performed with a custom-made hybrid FPGA-CPU infrastructure, essential for fast real-time generation of images, image analysis, decision-making, and sorting. Cells were sorted at a rate of ~100 eps based on the spectral and morphological information in their four-color SRS images. This constituted an increase of a few orders of magnitude in both information content and throughput compared to previous sorting methods, which sorted at 1 eps at best for spectrum-based automated sorters[24].

4. APPLICATIONS OF COHERENT RAMAN FLOW CYTOMETRY

A current challenge in cell biology is understanding the heterogeneity of individual cells. With the rise of single-cell next-generation sequencing techniques, single-cell analysis using genomics, epigenomics, transcriptomics, and proteomics has become widely available[52]. However, genomic and proteomic information, although essential, is incomplete without metabolomics. Current metabolomic approaches comprise mass spectroscopy (MS), nuclear magnetic resonance (NMR), and Raman spectroscopy. Single-cell MS techniques allow the measurement of hundreds of metabolites with high precision[53]. However, MS is destructive, hindering technique integration, longitudinal single-cell studies, and additional downstream analysis. NMR is non-destructive, but inherently slow[54]. On the other hand, fluorescence detection allows for high-throughput analysis, but often requires labels that may possess toxicity and interfere with cell homeostasis. For metabolomics to catch up with the other -omics, a high-throughput non-destructive technique is greatly needed. Raman spectroscopy is attractive for biological applications given its non-destructive, label-free, high-resolution nature. High-throughput Raman spectroscopy unlocks a plethora of new experiments to better understand the heterogeneous nature of single-cell populations, from single-cell analysis of microalgae[1–4] to marker-free cancer detection[3]. Here we discuss the main biological questions addressed by coherent Raman flow cytometry and extrapolate future biological questions that this novel approach could help elucidate.

4.1. Microbiology

Microalgae, yeast, and bacteria are resilient and can accumulate metabolites to high concentrations, making them ideal metabolomics model systems. In 2017, Zhang *et al*. detected single *Staphylococcus sp.* cells under flow using the high-wavenumber region, nonetheless the absence of microfluidic focusing meant only a small percentage of the bacteria could be detected[31]. Camp *et al*. reported high-throughput Raman flow cytometry of *Saccharomyces cerevisiae* cells, distinguishing two yeast subpopulations by both forward scattering and Raman spectrum[30] (Figure 3a). This approach only acquired eight spectral points over the whole spectra, detecting broad

changes in the high-wavenumber region and the fingerprint region[30]. At a higher resolution, Hiramatsu *et al*. reported a high-throughput FT-CARS Raman flow cytometry platform probing single *Haematococcus lacustris* and *Euglena gracilis* cells (Figure 3b)[1]. The system was sensitive to chlorophyll and carotenoid astaxanthin, whose signals were enhanced via the resonant Raman effect, as well as the β(1-3)-polysaccharide paramylon. The use of $^{13}CO_2$ allowed exploring the longitudinal dynamics of astaxantin production of *H. lacustris*, by analyzing the shift of the main astaxanthin Raman band due to isotope substitution[1]. The same system was used to investigate the paramylon metabolism of *E. gracilis* (Figure 3c).[2] Suzuki *et al.* performed multicolor imaging SRS Raman flow cytometry in the high-wavenumber region, detecting lipids, paramylon, and chlorophyll in *E. gracilis* cells. The single-cell SRS images allowed morphological classification by a neural network, showing >99% classification accuracy after 0, 10, and 58 days of growth (Figure 3d)[3]. Nitta *et al.* conducted SRS image-activated cell sorting of multiple microalgal species. *E. gracilis* cells grown in media containing ^{12}C and ^{13}C showed shifted paramylon peaks. Live-cell sorting was demonstrated sorting ^{13}C paramylon-rich *E. gracilis* cells from a mixed $^{12}C/^{13}C$ population and confirmed using FACS. Additionally, rare super-lipid-rich mutants were isolated and cloned from plasma mutated *Chlamydomonas sp.* KC4 cells, showing promising applications of high-throughput Raman cell sorting for directed evolution or selective breeding (Figure 3e)[4].

4.2. Lipid biology

The strongest Raman band from biological samples, other than the OH-stretching water band at 3420 cm^{-1}, lies in the high-wavenumber region (2800 - 3200 cm^{-1}) and is comprised primarily of CH-stretching. Lipids are rich in CH bonds, and multiple studies have targeted adipocytes for this reason. For example, Wang *et al*. used their CARS flow cytometer to analyze the ν_s CH_2-vibration band at 2840 cm^{-1} for detecting and sizing mammary tissue mouse adipocytes (Figure 4a)[28]. Similarly, Zhang *et al*. targeted the region between 2900 and 3100 cm^{-1} with their multiplex SRS flow cytometer[31], acquiring spectra from differentiated and non-differentiated 3T3-L1 murine adipocytes (Figure 4b). These cells show fibroblast morphology in the non-differentiated state and accumulation of lipids in lipid droplets after insulin-induced differentiation. Zhang *et al.* showed differences based on the 2940 and 2850 cm^{-1} bands, with clustering between the two groups[31]. Likewise, Nitta *et al.* used their Raman image-activated cell sorter to track lipids and proteins during the differentiation of 3T3-L1 embryonic mouse cells towards adipocyte-like cells. Specifically, they demonstrated a 3.8x enrichment of lipid-droplet-rich cells via cell sorting, with 74% of the cells in the sorted channel possessing lipid droplets compared to just 20% of the cells in the unsorted channel (Figure 4c)[4].

4.3. Cancer detection

The past two decades have seen an increasing interest in the development of liquid biopsy techniques for the detection of circulating tumor cells (CTCs) in blood[55]. CTCs, discovered in 1869, are cells that have entered blood vessels from a primary tumor, circulate in the body, and can lead to the development of secondary metastases at distant locations. They appear in the blood at concentrations of 1-10 CTCs per mL of blood. The detection of CTCs holds promise for monitoring cancer progression and determining therapeutic strategies. However, the expression of the cell surface glycoprotein conventionally used as a biomarker for fluorescence detection, epithelial cell adhesion molecule (EpCAM), can disappear through the epithelial-to-mesenchymal transition[55]. Therefore, it is important to detect and enumerate CTCs in blood at high throughput without the need for fluorescent labeling. Coherent Raman flow cytometry is suitable for addressing this need. For example, Suzuki *et al.* used multicolor SRS imaging Raman flow cytometry to acquire four different Raman bands in the CH-stretching region (2860, 2910, 2937, and 3040 cm^{-1}) for cancer detection (Figure 4d). They showed the system capabilities on a liquid biopsy model system, with >93% accuracy on the classification of red blood cells, Jurkat cells, HT29 cells, and peripheral blood mononuclear cells. Furthermore, they demonstrated accurate

detection of spiked cancer cells in lysed blood, showing the potential of high-throughput label-free liquid biopsy[3].

4.4. Cell therapies

By virtue of its ability to evaluate cells in a high-throughput and label-free manner, coherent Raman flow cytometry is highly effective for screening cells such as those used in cell therapy. Specifically, human induced pluripotent stem cells (hiPSCs) and CAR-T cells cannot be fluorescently labeled before injecting them to the human body as therapeutic agents because fluorescent labeling can lead to immunogenicity and introduce xenobiotic compounds[21,22]. Nitta *et al*. imaged naïve and primed hiPSCs under flow showing differences in the localization of carbohydrate and proteins[4]. An increased carbohydrate content in primed hiPSCs was confirmed with SRS microscopy as a biomarker for the primed state (Figure 4e).

5. FUTURE OPPORTUNITIES AND CHALLENGES OF COHERENT RAMAN FLOW CYTOMETRY

Coherent Raman flow cytometry has shown versatility for single-cell studies. However, challenges remain, including increasing sensitivity, throughput, and sorting capabilities. Additionally, further integration with advanced techniques such as droplet microfluidics and machine learning could increase the range of applications of the current platforms. Their sensitivity to isotope-labelled molecules make coherent Raman flow cytometry a good approach for finding metabolically active cells from large cell populations with minimal effects on cell metabolism. Future clinical applications could include *in vivo* measurement capabilities given its non-destructive nature. Here we discuss these future opportunities and technical challenges.

5.1. Toward higher sensitivity

The biggest challenge in Raman flow cytometry is its low sensitivity compared to fluorescence flow cytometry, where the detection of biomolecules at the level of 100 molecules/cell is routinely performed with throughputs higher than 100,000 eps, with the caveat that suitable fluorescence probes are available for the target molecules. On the other hand, the detection limit of Raman spectroscopy is on the molar to millimolar level[56], which is orders of magnitude less sensitive than fluorescence detection. Consequently, Raman flow cytometry generally targets concentrated metabolites such as lipids, proteins, and carbohydrates. For instance, Suzuki *et al*. and Nitta *et al*.'s Raman imaging flow cytometry and sorting have been major achievements for Raman flow cytometry, but are limited to a 4-color detection targeting the high-wavenumber region. Fingerprint Raman flow cytometry and sorting are yet to be reported. Additionally, fingerprint analysis of mammalian cells is still out of reach for Raman flow cytometry methods due to the generally weaker signal of mammalian cells in this region. Unlocking Raman flow cytometry in the fingerprint region would allow for nucleic acid, carbohydrates, proteins, and lipids discrimination, challenging when using only the high-wavenumber information. To overcome this limitation, different methods for enhancing the detection sensitivity of Raman spectroscopy have been proposed and demonstrated for both spontaneous and CRS. For CRS, it has been reported that the sensitivity can be enhanced by using heterodyne detection[42,57–60], polarization-selective measurements[58,59], and pulse shaping[60], all promising approaches for Raman flow cytometry. Alternatively, the use of Raman tags can enhance the sensitivity down to the micromolar level with electronic resonance enhancement[61]. Although this approach sacrifices the label-free nature of Raman flow cytometry, it has the potential to beat the color barrier in conventional fluorescence flow cytometry thanks to the narrow width of Raman bands[61].

5.2. Toward higher analysis throughput

The throughput of the reported Raman flow cytometers is on the order of 100 - 1,000 eps[1,31], still a few orders of magnitude lower than that of commercially available fluorescence flow cytometers (~100,000 eps). Unfortunately, increasing throughput simply by increasing the flow speed would not be effective because it would sacrifice Raman detection sensitivity. Smart integration of microfluidics and optics is necessary for reducing dead time during which no cell is interrogated. Deblurring techniques developed in the context of imaging flow cytometry, such as the virtual-freezing method[62], will be useful to increase the effective signal integration time without compromising the flow rate. Also, microfluidic focusing improvements can be implemented to increase the efficiency of the flow cytometry measurements. Alternatively, throughput can be increased by using parallel microfluidic devices combined with wide-field sensing, which has already been applied to high-throughput fluorescence imaging flow cytometry[63,64]. In the case of Raman spectroscopy, a combination of parallel fluidics with multi-focus Raman detection[65] could increase throughput by an order of magnitude.

5.3. Toward higher sorting throughput

The highest sorting throughput in Raman flow cytometry to date is about 100 eps[4]. For realizing higher sorting throughput, in addition to the enhancement of Raman detection sensitivity as described above, seamless integration of optics, microfluidics, and signal processing is needed. Specifically, for coherent Raman-activated cell sorting, spectral acquisition and sorting decision-making need to be completed in less than ~1 ms. On the microfluidics side, reduction of the sorting window is crucial for realizing high throughput without compromising sorting purity and yield[4]. Surface acoustic waves, dielectrophoresis, and membrane pumps have been reported as cell sorting methodologies. Recently, cell sorting with the use of laser-induced cavitation bubbles demonstrated an unprecedentedly narrow sorting window down to ~10 μm at a flow speed of 1 m/s[66]. Additionally, some sorting methods can compromise cell viability[67]. An appropriate sorting method should be chosen based on target-cell characteristics.

5.4. Integration with droplet microfluidics

Droplet microfluidics allows compartmentalization of the target cells in tens to hundreds of micrometer water-in-oil droplets[68]. Droplets can be easily sorted using dielectrophoresis and are a promising approach for Raman-activated cell sorting. A notable advantage of using microdroplets in cell sorting is within-droplet culturing of the sorted cells under an isolated environment, enabling the analysis of cellular secretion and proliferation ability[69]. For example, Isozaki *et al*. demonstrated high-throughput (>1,000 eps) sorting of large (>100 pL) droplets with a sequentially addressable dielectrophoretic array[68]. Large-droplet sorting enables long-term monitoring of cells based on various phenotypes such as their growth rate. Spontaneous Raman-activated droplet sorting with a throughput of about 2 eps for label-free screening based on yeast enzyme function was demonstrated[70]. Combining droplet microfluidics and coherent Raman flow cytometry is expected to significantly enhance the throughput of Raman-activated droplet sorting.

5.5. Integration with machine learning

The interpretation of spectral data obtained in Raman flow cytometry has generally been based on Raman intensity at specific Raman shifts[1,4,31] primarily because the cellular spectral and spatial features are not very complicated. Although Raman-intensity-based analysis works well for the quantification of relatively small molecules with distinct spectral profiles such as metabolites, the differences in spectral signatures for different types of cells are often subtle, making Raman-intensity-based analysis insufficient. Recently, machine-learning based analysis has proven to be a powerful tool for the discrimination of close cell types[71]. As the machine-learning approach requires the preparation of large amounts of training data for reliable classification, integration

of machine learning methods and high-throughput Raman flow cytometry datasets is expected to boost the accuracy of Raman-based cell type classification.

5.6. In vivo flow cytometry

So far, Raman flow cytometry has been performed *ex vivo*, with cells extracted from the human body and measured in an artificial flow stream. However, in hematological applications, direct *in vivo* flow cytometry of blood cells is desirable to minimize potential error and bias associated with sample preparation and time-dependent measurement. *In vivo* Raman flow cytometry, in which signals from bloodstream cells are measured, is a promising alternative to *ex vivo* analysis[72]. For example, single-color *in vivo* Raman imaging flow cytometry with SRS has been demonstrated for detecting red blood cells flowing in a thin mouse ear capillary – with a typical thickness of a few hundred micrometers[73]. For its application to blood vessels at different locations, however, deeper optical penetration depth is necessary. A technical challenge in deep-tissue imaging is wavefront distortion, which is detrimental for nonlinear Raman signal generation because it lowers photon flux at the interrogation point. Though adaptive optics have proven to be a powerful method for compensating wavefront distortion in fluorescence imaging[74], its application to nonlinear Raman imaging is not straightforward because it necessitates the precise control of two wavefronts (pump and Stokes) that may be spectrally broadband. Alternatively, Raman flow cytometry could make use of the recently demonstrated deep-tissue nonlinear Raman imaging techniques using Bessel beams, whose beam profile is less affected by diffraction in biological tissues[75].

6. CONCLUSIONS

The integration of the state-of-the-art CRS and microfluidics technology has enabled high-throughput single-cell analysis in a label-free manner. SRS and CARS have been the main CRS techniques used in Raman flow cytometry. During the last decade, new Raman flow cytometry techniques have arisen such as MCARS, FT-CARS, SRS imaging flow cytometry and SRS imaging cell sorting. As a platform, microfluidics with hydrodynamic and acoustic focusing have improved the single-cell acquisition, and coherent Raman flow cytometry has enabled label-free biological applications such as microbial screening, cell differentiation tracking or cancer detection. Despite progress in the field, challenges remain in the improvement of sensitivity, spectral resolution and bandwidth, cell flow focusing and dead time, and real-time decision making/machine learning integration. Due to the multidisciplinary nature of Raman flow cytometry, these challenges will be tackled by innovations in different areas including laser science, photonics, microfluidics, computer science, molecular engineering, and biomedicine. As a growing field, high-throughput Raman flow cytometry and Raman-activated cell sorting are promising techniques for label-free metabolic analysis of single cells.

AUTHOR INFORMATION

Corresponding Author

* Keisuke Goda – ORCID iD: https://orcid.org/0000-0001-6302-6038 **E-mail**: goda@chem.s.u-tokyo.ac.jp

Authors

Julia Gala de Pablo – ORCID iD: https://orcid.org/0000-0003-0557-9632

Matthew Lindley – ORCID iD: https://orcid.org/0000-0002-8164-8479

Kotaro Hiramatsu – ORCID iD: https://orcid.org/0000-0003-0767-019X

Author Contributions

The manuscript was written through contributions of all authors. All authors have given approval to the final version of the manuscript.

Notes

Keisuke Goda is a shareholder of CYBO and Cupido. The other authors declare no competing financial interest.

Biographies

Julia Gala de Pablo obtained her Ph.D. degree in physics from the University of Leeds in 2019 and is a postdoctoral fellow of the Japan Society for the Promotion of Science (JSPS) working at the University of Tokyo.

Matthew Lindley obtained his M.S. degree in chemistry from the University of Tokyo in 2018 and is a Ph.D. student in the Department of Chemistry at the University of Tokyo.

Kotaro Hiramatsu obtained his Ph.D. degree in chemistry from the University of Tokyo in 2016 and is an assistant professor in the Department of Chemistry at the University of Tokyo.

Keisuke Goda is a professor in the Department of Chemistry at the University of Tokyo in Japan, an adjunct professor at the Institute of Technological Sciences at Wuhan University in China, and an adjunct professor in the Department of Bioengineering at the University of California, Los Angeles in the United States of America. He obtained a B.S. degree from the University of California, Berkeley in 2001 and a Ph.D. degree from Massachusetts Institute of Technology in 2007, both in physics. After several years of work at California Institute of Technology and the University of California, Los Angeles, he joined the University of Tokyo in 2012.

ACKNOWLEDGEMENT

This work was supported by the JSPS Core-to-Core Program, JSPS KAKENHI, White Rock Foundation, KISTEC, Ogasawara Foundation, Takeda Science Foundation, Kurita Foundation, Nakatani Foundation, and Cupido. J. G. P. thanks JSPS for the standard research fellowship and the grant-in-aid.

REFERENCES

(1) Hiramatsu, K.; Ideguchi, T.; Yonamine, Y.; Lee, S.; Luo, Y.; Hashimoto, K.; Ito, T.; Hase, M.; Park, J.-W.; Kasai, Y.; Sakuma, S.; Hayakawa, T.; Arai, F.; Hoshino, Y.; Goda, K. High-Throughput Label-Free Molecular Fingerprinting Flow Cytometry. *Science Advances* **2019**, *5*, eaau0241. https://doi.org/10/ggtkm4.

(2) Hiramatsu, K.; Yamada, K.; Lindley, M.; Suzuki, K.; Goda, K. Large-Scale Label-Free Single-Cell Analysis of Paramylon in Euglena Gracilis by High-Throughput Broadband Raman Flow Cytometry. *Biomedical Optics Express* **2020**, *11*, 1752. https://doi.org/10/gg4bx5.

(3) Suzuki, Y.; Kobayashi, K.; Wakisaka, Y.; Deng, D.; Tanaka, S.; Huang, C.-J.; Lei, C.; Sun, C.-W.; Liu, H.; Fujiwaki, Y.; Lee, S.; Isozaki, A.; Kasai, Y.; Hayakawa, T.; Sakuma, S.; Arai, F.; Koizumi, K.; Tezuka, H.; Inaba, M.; Hiraki, K.; Ito, T.; Hase, M.; Matsusaka, S.; Shiba, K.; Suga, K.; Nishikawa, M.; Jona, M.; Yatomi, Y.; Yalikun, Y.; Tanaka, Y.; Sugimura, T.; Nitta, N.; Goda, K.; Ozeki, Y. Label-Free Chemical Imaging Flow Cytometry by High-Speed Multicolor Stimulated Raman Scattering. *PNAS* **2019**, *116*, 15842–15848. https://doi.org/10/ggspvm.

(4) Nitta, N.; Iino, T.; Isozaki, A.; Yamagishi, M.; Kitahama, Y.; Sakuma, S.; Suzuki, Y.; Tezuka, H.; Oikawa, M.; Arai, F.; Asai, T.; Deng, D.; Fukuzawa, H.; Hase, M.; Hasunuma, T.; Hayakawa, T.; Hiraki, K.; Hiramatsu, K.; Hoshino, Y.; Inaba, M.; Inoue, Y.; Ito, T.; Kajikawa, M.; Karakawa, H.; Kasai, Y.; Kato, Y.; Kobayashi, H.; Lei, C.; Matsusaka, S.; Mikami, H.; Nakagawa, A.; Numata, K.; Ota, T.; Sekiya, T.; Shiba, K.; Shirasaki, Y.; Suzuki, N.; Tanaka, S.; Ueno, S.; Watarai, H.; Yamano, T.; Yazawa, M.; Yonamine, Y.; Di Carlo, D.; Hosokawa, Y.; Uemura, S.; Sugimura, T.; Ozeki, Y.; Goda, K. Raman Image-Activated Cell Sorting. *Nature Communications* **2020**, *11*, 3452. https://doi.org/10/gg5dd2.

(5) Léonard, L.; Bouarab Chibane, L.; Ouled Bouhedda, B.; Degraeve, P.; Oulahal, N. Recent Advances on Multi-Parameter Flow Cytometry to Characterize Antimicrobial Treatments. *Front. Microbiol.* **2016**, *7*. https://doi.org/10/ghw9b5.

(6) Renner, T. M.; Tang, V. A.; Burger, D.; Langlois, M.-A. Intact Viral Particle Counts Measured by Flow Virometry Provide Insight into the Infectivity and Genome Packaging Efficiency of Moloney Murine Leukemia Virus. *J Virol* **2019**, *94*, e01600-19, /jvi/94/2/JVI.01600-19.atom. https://doi.org/10/gjf82z.
(7) Aebisher, D.; Bartusik, D.; Tabarkiewicz, J. Laser Flow Cytometry as a Tool for the Advancement of Clinical Medicine. *Biomedicine & Pharmacotherapy* **2017**, *85*, 434–443. https://doi.org/10.1016/j.biopha.2016.11.048.
(8) Greve, B.; Kelsch, R.; Spaniol, K.; Eich, H. T.; Götte, M. Flow Cytometry in Cancer Stem Cell Analysis and Separation. *Cytometry Part A* **2012**, *81A*, 284–293. https://doi.org/10/gjf8tr.
(9) Pereira, H.; Schulze, P. S. C.; Schüler, L. M.; Santos, T.; Barreira, L.; Varela, J. Fluorescence Activated Cell-Sorting Principles and Applications in Microalgal Biotechnology. *Algal Research* **2018**, *30*, 113–120. https://doi.org/10/gjf8x9.
(10) Han, Y.; Gu, Y.; Zhang, A. C.; Lo, Y.-H. Review: Imaging Technologies for Flow Cytometry. *Lab Chip* **2016**, *16*, 4639–4647. https://doi.org/10/ggwffx.
(11) Dam, P. A. van; Watson, J. V.; Lowe, D. G.; Chard, T.; Shepherd, J. H. Comparative Evaluation of Fresh, Fixed, and Cryopreserved Solid Tumor Cells for Reliable Flow Cytometry of DNA and Tumor Associated Antigen. *Cytometry* **1992**, *13*, 722–729. https://doi.org/10/bsjvz5.
(12) Picot, J.; Guerin, C. L.; Le Van Kim, C.; Boulanger, C. M. Flow Cytometry: Retrospective, Fundamentals and Recent Instrumentation. *Cytotechnology* **2012**, *64*, 109–130. https://doi.org/10/fz3jfn.
(13) Radbruch, A. *Flow Cytometry and Cell Sorting*; Springer Science & Business Media, 2013.
(14) Shapiro, H. M. *Practical Flow Cytometry*; John Wiley & Sons, 2005.
(15) Wei, L.; Hu, F.; Chen, Z.; Shen, Y.; Zhang, L.; Min, W. Live-Cell Bioorthogonal Chemical Imaging: Stimulated Raman Scattering Microscopy of Vibrational Probes. *Acc. Chem. Res.* **2016**, *49*, 1494–1502. https://doi.org/10/f8xph6.
(16) Park, S.; Reyer, M. A.; McLean, E. L.; Liu, W.; Fei, J. An Improved Method for Bacterial Immunofluorescence Staining To Eliminate Antibody Exclusion from the Fixed Nucleoid. *Biochemistry* **2019**, *58*, 4457–4465. https://doi.org/10/gjf8x6.
(17) Hulspas, R.; O'Gorman, M. R. G.; Wood, B. L.; Gratama, J. W.; Sutherland, D. R. Considerations for the Control of Background Fluorescence in Clinical Flow Cytometry. *Cytometry Part B: Clinical Cytometry* **2009**, *76B*, 355–364. https://doi.org/10/dfpj3q.
(18) Fajrial, A. K.; He, Q. Q.; Wirusanti, N. I.; Slansky, J. E.; Ding, X. A Review of Emerging Physical Transfection Methods for CRISPR/Cas9-Mediated Gene Editing. *Theranostics* **2020**, *10*, 5532–5549. https://doi.org/10/ghtdp2.
(19) Alamudi, S. H.; Satapathy, R.; Kim, J.; Su, D.; Ren, H.; Das, R.; Hu, L.; Alvarado-Martínez, E.; Lee, J. Y.; Hoppmann, C.; Peña-Cabrera, E.; Ha, H.-H.; Park, H.-S.; Wang, L.; Chang, Y.-T. Development of Background-Free Tame Fluorescent Probes for Intracellular Live Cell Imaging. *Nature Communications* **2016**, *7*, 11964. https://doi.org/10/gjf8q9.
(20) Tuchin, V. V.; Tárnok, A.; Zharov, V. P. In Vivo Flow Cytometry: A Horizon of Opportunities. *Cytometry Part A* **2011**, *79A*, 737–745. https://doi.org/10/dpg85x.
(21) George, B. Regulations and Guidelines Governing Stem Cell Based Products: Clinical Considerations. *Perspect Clin Res* **2011**, *2*, 94–99. https://doi.org/10/dtf3mv.
(22) Marks, P. The FDA's Regulatory Framework for Chimeric Antigen Receptor-T Cell Therapies. *Clin Transl Sci* **2019**, *12*, 428–430. https://doi.org/10/gh7khx.
(23) Jett, J. H. Raman Spectroscopy Comes to Flow Cytometry. *Cytometry Part A* **2008**, *73A*, 109–110. https://doi.org/10/bxcvps.
(24) Song, Y.; Yin, H.; Huang, W. E. Raman Activated Cell Sorting. *Current Opinion in Chemical Biology* **2016**, *33*, 1–8. https://doi.org/10/ggzgkk.
(25) *Coherent Raman Scattering Microscopy*; Cheng, J.-X., Xie, X. S., Eds.; Series in cellular and clinical imaging; CRC Press, Taylor & Francis Group: Boca Raton, 2013.
(26) Evans, C. L.; Potma, E. O.; Puoris'haag, M.; Côté, D.; Lin, C. P.; Xie, X. S. Chemical Imaging of Tissue in Vivo with Video-Rate Coherent Anti-Stokes Raman Scattering Microscopy. *PNAS* **2005**, *102*, 16807–16812. https://doi.org/10/cvdz6n.
(27) Hu, F.; Shi, L.; Min, W. Biological Imaging of Chemical Bonds by Stimulated Raman Scattering Microscopy. *Nat Methods* **2019**, *16*, 830–842. https://doi.org/10.1038/s41592-019-0538-0.

(28) Wang, H.-W.; Bao, N.; Le, T. L.; Lu, C.; Cheng, J.-X. Microfluidic CARS Cytometry. *Opt. Express* **2008**, *16*, 5782. https://doi.org/10/dxx58z.

(29) Camp Jr., C. H.; Yegnanarayanan, S.; Eftekhar, A. A.; Sridhar, H.; Adibi, A. Multiplex Coherent Anti-Stokes Raman Scattering (MCARS) for Chemically Sensitive, Label-Free Flow Cytometry. *Opt. Express* **2009**, *17*, 22879. https://doi.org/10/dvwkhf.

(30) Camp, C. H.; Yegnanarayanan, S.; Eftekhar, A. a; Adibi, A. Label-Free Flow Cytometry Using Multiplex Coherent Anti-Stokes Raman Scattering (MCARS) for the Analysis of Biological Specimens. *Optics letters* **2011**, *36*, 2309–2311. https://doi.org/10/ddj33n.

(31) Zhang, C.; Huang, K.-C.; Rajwa, B.; Li, J.; Yang, S.; Lin, H.; Liao, C.; Eakins, G.; Kuang, S.; Patsekin, V.; Robinson, J. P.; Cheng, J.-X. Stimulated Raman Scattering Flow Cytometry for Label-Free Single-Particle Analysis. *Optica* **2017**, *4*, 103. https://doi.org/10/ggtk7p.

(32) Camp Jr, C. H.; Cicerone, M. T. Chemically Sensitive Bioimaging with Coherent Raman Scattering. *Nature Photonics* **2015**, *9*, 295–305. https://doi.org/10.1038/nphoton.2015.60.

(33) Ivleva, N. P.; Kubryk, P.; Niessner, R. Raman Microspectroscopy, Surface-Enhanced Raman Scattering Microspectroscopy, and Stable-Isotope Raman Microspectroscopy for Biofilm Characterization. *Analytical and Bioanalytical Chemistry* **2017**, *409*, 4353–4375. https://doi.org/10/b52s.

(34) Prince, R. C.; Frontiera, R. R.; Potma, E. O. Stimulated Raman Scattering: From Bulk to Nano. *Chem Rev* **2017**, *117*, 5070–5094. https://doi.org/10/gf853r.

(35) Maker, P. D.; Terhune, R. W. Study of Optical Effects Due to an Induced Polarization Third Order in the Electric Field Strength. *Phys. Rev.* **1965**, *137*, A801–A818. https://doi.org/10.1103/PhysRev.137.A801.

(36) Ando, T.; Xuan, W.; Xu, T.; Dai, T.; Sharma, S. K.; Kharkwal, G. B.; Huang, Y.-Y.; Wu, Q.; Whalen, M. J.; Sato, S.; Obara, M.; Hamblin, M. R. Comparison of Therapeutic Effects between Pulsed and Continuous Wave 810-Nm Wavelength Laser Irradiation for Traumatic Brain Injury in Mice. *PLoS One* **2011**, *6*. https://doi.org/10/d737xt.

(37) Freudiger, C. W.; Min, W.; Saar, B. G.; Lu, S.; Holtom, G. R.; He, C.; Tsai, J. C.; Kang, J. X.; Xie, X. S. Label-Free Biomedical Imaging with High Sensitivity by Stimulated Raman Scattering Microscopy. *Science* **2008**, *322*, 1857–1861. https://doi.org/10/c83dds.

(38) Réhault, J.; Crisafi, F.; Kumar, V.; Ciardi, G.; Marangoni, M.; Cerullo, G.; Polli, D. Broadband Stimulated Raman Scattering with Fourier-Transform Detection. *Opt. Express* **2015**, *23*, 25235. https://doi.org/10/gdm9sf.

(39) Wakisaka, Y.; Suzuki, Y.; Iwata, O.; Nakashima, A.; Ito, T.; Hirose, M.; Domon, R.; Sugawara, M.; Tsumura, N.; Watarai, H.; Shimobaba, T.; Suzuki, K.; Goda, K.; Ozeki, Y. Probing the Metabolic Heterogeneity of Live Euglena Gracilis with Stimulated Raman Scattering Microscopy. *Nature Microbiology* **2016**, *1*, 16124. https://doi.org/10/gf853j.

(40) Cheng, J.; Volkmer, A.; Book, L. D.; Xie, X. S. Multiplex Coherent Anti-Stokes Raman Scattering Microspectroscopy and Study of Lipid Vesicles. *J. Phys. Chem. B* **2002**, *106*, 8493–8498. https://doi.org/10/dbpcwk.

(41) Kano, H.; Hamaguchi, H. Vibrationally Resonant Imaging of a Single Living Cell by Supercontinuum-Based Multiplex Coherent Anti-Stokes Raman Scattering Microspectroscopy. *Opt. Express, OE* **2005**, *13*, 1322–1327. https://doi.org/10/d764kr.

(42) Evans, C. L.; Potma, E. O.; Xie, X. S. Coherent Anti-Stokes Raman Scattering Spectral Interferometry: Determination of the Real and Imaginary Components of Nonlinear Susceptibility X^(3) for Vibrational Microscopy. *Opt. Lett.* **2004**, *29*, 2923. https://doi.org/10/bjcghr.

(43) Vartiainen, E. M. Phase Retrieval Approach for Coherent Anti-Stokes Raman Scattering Spectrum Analysis. *J. Opt. Soc. Am. B, JOSAB* **1992**, *9*, 1209–1214. https://doi.org/10/b2ktw9.

(44) Liu, Y.; Lee, Y. J.; Cicerone, M. T. Broadband CARS Spectral Phase Retrieval Using a Time-Domain Kramers–Kronig Transform. *Opt. Lett., OL* **2009**, *34*, 1363–1365. https://doi.org/10/cckbwq.

(45) Ogilvie, J. P.; Cui, M.; Pestov, D.; Sokolov, A. V.; Scully, M. O. Time-Delayed Coherent Raman Spectroscopy. *Molecular Physics* **2008**, *106*, 587–594. https://doi.org/10/b33mvw.

(46) Prince, B. D.; Chakraborty, A.; Prince, B. M.; Stauffer, H. U. Development of Simultaneous Frequency- and Time-Resolved Coherent Anti-Stokes Raman Scattering for Ultrafast Detection of Molecular Raman Spectra. *J. Chem. Phys.* **2006**, *125*, 044502. https://doi.org/10/b2rkw8.

(47) Cui, M.; Joffre, M.; Skodack, J.; Ogilvie, J. P. Interferometric Fourier Transform Coherent Anti-Stokes Raman Scattering. *Optics Express* **2006**, *14*, 8448. https://doi.org/10/bxj2ct.
(48) Hashimoto, K.; Takahashi, M.; Ideguchi, T.; Goda, K. Broadband Coherent Raman Spectroscopy Running at 24,000 Spectra per Second. *Scientific Reports* **2016**, *6*, 21036. https://doi.org/10/f79dp9.
(49) Tamamitsu, M.; Sakaki, Y.; Nakamura, T.; Podagatlapalli, G. K.; Ideguchi, T.; Goda, K. Ultrafast Broadband Fourier-Transform CARS Spectroscopy at 50,000 Spectra/s Enabled by a Scanning Fourier-Domain Delay Line. *Vibrational Spectroscopy* **2017**, *91*, 163–169. https://doi.org/10/gbmpqz.
(50) Petersson, F.; Nilsson, A.; Jönsson, H.; Laurell, T. Carrier Medium Exchange through Ultrasonic Particle Switching in Microfluidic Channels. *Anal. Chem.* **2005**, *77*, 1216–1221. https://doi.org/10/d32pfw.
(51) Sakuma, S.; Kasai, Y.; Hayakawa, T.; Arai, F. On-Chip Cell Sorting by High-Speed Local-Flow Control Using Dual Membrane Pumps. *Lab Chip* **2017**, *17*, 2760–2767. https://doi.org/10/gjf8zt.
(52) Goldman, S. L.; MacKay, M.; Afshinnekoo, E.; Melnick, A. M.; Wu, S.; Mason, C. E. The Impact of Heterogeneity on Single-Cell Sequencing. *Front. Genet.* **2019**, *10*. https://doi.org/10/gg99jm.
(53) Evers, T. M. J.; Hochane, M.; Tans, S. J.; Heeren, R. M. A.; Semrau, S.; Nemes, P.; Mashaghi, A. Deciphering Metabolic Heterogeneity by Single-Cell Analysis. *Anal. Chem.* **2019**, *91*, 13314–13323. https://doi.org/10/gg4bxg.
(54) Giraudeau, P. NMR-Based Metabolomics and Fluxomics: Developments and Future Prospects. *Analyst* **2020**, *145*, 2457–2472. https://doi.org/10/ghbjd4.
(55) Lin, E.; Cao, T.; Nagrath, S.; King, M. R. Circulating Tumor Cells: Diagnostic and Therapeutic Applications. *Annual Review of Biomedical Engineering* **2018**, *20*, 329–352. https://doi.org/10/gjf8wx.
(56) Cheng, J.-X.; Xie, X. S. Vibrational Spectroscopic Imaging of Living Systems: An Emerging Platform for Biology and Medicine. *Science* **2015**, *350*. https://doi.org/10/gf852g.
(57) Potma, E. O.; Evans, C. L.; Xie, X. S. Heterodyne Coherent Anti-Stokes Raman Scattering (CARS) Imaging. *Opt. Lett.* **2006**, *31*, 241. https://doi.org/10/b3s3vg.
(58) Oron, D.; Dudovich, N.; Silberberg, Y. Femtosecond Phase-and-Polarization Control for Background-Free Coherent Anti-Stokes Raman Spectroscopy. *Phys. Rev. Lett.* **2003**, *90*, 213902. https://doi.org/10/cp4zh2.
(59) Littleton, B.; Kavanagh, T.; Festy, F.; Richards, D. Spectral Interferometric Implementation with Passive Polarization Optics of Coherent Anti-Stokes Raman Scattering. *Phys. Rev. Lett.* **2013**, *111*, 103902. https://doi.org/10/gjf8w3.
(60) Dudovich, N.; Oron, D.; Silberberg, Y. Single-Pulse Coherent Anti-Stokes Raman Spectroscopy in the Fingerprint Spectral Region. *The Journal of Chemical Physics* **2003**, *118*, 9208–9215. https://doi.org/10/fs66pq.
(61) Hu, F.; Zeng, C.; Long, R.; Miao, Y.; Wei, L.; Xu, Q.; Min, W. Supermultiplexed Optical Imaging and Barcoding with Engineered Polyynes. *Nature Methods* **2018**, *15*, 194–200. https://doi.org/10/gcttww.
(62) Mikami, H.; Kawaguchi, M.; Huang, C.-J.; Matsumura, H.; Sugimura, T.; Huang, K.; Lei, C.; Ueno, S.; Miura, T.; Ito, T.; Nagasawa, K.; Maeno, T.; Watarai, H.; Yamagishi, M.; Uemura, S.; Ohnuki, S.; Ohya, Y.; Kurokawa, H.; Matsusaka, S.; Sun, C.-W.; Ozeki, Y.; Goda, K. Virtual-Freezing Fluorescence Imaging Flow Cytometry. *Nature Communications* **2020**, *11*, 1162. https://doi.org/10/ghbzrt.
(63) Rane, A. S.; Rutkauskaite, J.; deMello, A.; Stavrakis, S. High-Throughput Multi-Parametric Imaging Flow Cytometry. *Chem* **2017**, *3*, 588–602. https://doi.org/10/gjfvn9.
(64) Piyasena, M. E.; Austin Suthanthiraraj, P. P.; Applegate, R. W.; Goumas, A. M.; Woods, T. A.; López, G. P.; Graves, S. W. Multinode Acoustic Focusing for Parallel Flow Cytometry. *Anal. Chem.* **2012**, *84*, 1831–1839. https://doi.org/10/fxw7th.
(65) Okuno, M.; Hamaguchi, H. Multifocus Confocal Raman Microspectroscopy for Fast Multimode Vibrational Imaging of Living Cells. *Opt. Lett.* **2010**, *35*, 4096. https://doi.org/10/c59z7c.
(66) Iino, T.; Okano, K.; Lee, S. W.; Yamakawa, T.; Hagihara, H.; Hong, Z.-Y.; Maeno, T.; Kasai, Y.; Sakuma, S.; Hayakawa, T.; Arai, F.; Ozeki, Y.; Goda, K.; Hosokawa, Y. High-Speed Microparticle Isolation Unlimited by Poisson Statistics. *Lab Chip* **2019**, *19*, 2669–2677. https://doi.org/10/gjf8vg.
(67) Shields, C. W.; Reyes, C. D.; López, G. P. Microfluidic Cell Sorting: A Review of the Advances in the Separation of Cells from Debulking to Rare Cell Isolation. *Lab Chip* **2015**, *15*, 1230–1249. https://doi.org/10/f66zmj.

(68) Isozaki, A.; Nakagawa, Y.; Loo, M. H.; Shibata, Y.; Tanaka, N.; Setyaningrum, D. L.; Park, J.-W.; Shirasaki, Y.; Mikami, H.; Huang, D.; Tsoi, H.; Riche, C. T.; Ota, T.; Miwa, H.; Kanda, Y.; Ito, T.; Yamada, K.; Iwata, O.; Suzuki, K.; Ohnuki, S.; Ohya, Y.; Kato, Y.; Hasunuma, T.; Matsusaka, S.; Yamagishi, M.; Yazawa, M.; Uemura, S.; Nagasawa, K.; Watarai, H.; Carlo, D. D.; Goda, K. Sequentially Addressable Dielectrophoretic Array for High-Throughput Sorting of Large-Volume Biological Compartments. *Science Advances* **2020**, *6*, eaba6712. https://doi.org/10/gh28m6.

(69) Mazutis, L.; Gilbert, J.; Ung, W. L.; Weitz, D. A.; Griffiths, A. D.; Heyman, J. A. Single-Cell Analysis and Sorting Using Droplet-Based Microfluidics. *Nat Protoc* **2013**, *8*, 870–891. https://doi.org/10/f4v347.

(70) Wang, X.; Xin, Y.; Ren, L.; Sun, Z.; Zhu, P.; Ji, Y.; Li, C.; Xu, J.; Ma, B. Positive Dielectrophoresis–Based Raman-Activated Droplet Sorting for Culture-Free and Label-Free Screening of Enzyme Function in Vivo. *Sci. Adv.* **2020**, *6*, eabb3521. https://doi.org/10/gg7f9k.

(71) Pavillon, N.; Hobro, A. J.; Akira, S.; Smith, N. I. Noninvasive Detection of Macrophage Activation with Single-Cell Resolution through Machine Learning. *Proc Natl Acad Sci U S A* **2018**, *115*, E2676–E2685. https://doi.org/10/gc8css.

(72) Biris, A. S.; Galanzha, E. I.; Li, Z.; Mahmood, M.; Xu, Y.; Zharov, V. P. In Vivo Raman Flow Cytometry for Real-Time Detection of Carbon Nanotube Kinetics in Lymph, Blood, and Tissues. *JBO* **2009**, *14*, 021006. https://doi.org/10/cgk6hk.

(73) Saar, B. G.; Freudiger, C. W.; Reichman, J.; Stanley, C. M.; Holtom, G. R.; Xie, X. S. Video-Rate Molecular Imaging in Vivo with Stimulated Raman Scattering. *Science* **2010**, *330*, 1368–1370. https://doi.org/10/dwgqxw.

(74) Ji, N.; Milkie, D. E.; Betzig, E. Adaptive Optics via Pupil Segmentation for High-Resolution Imaging in Biological Tissues. *Nature Methods* **2010**, *7*, 141–147. https://doi.org/10/bhnsns.

(75) Chen, X.; Zhang, C.; Lin, P.; Huang, K.-C.; Liang, J.; Tian, J.; Cheng, J.-X. Volumetric Chemical Imaging by Stimulated Raman Projection Microscopy and Tomography. *Nature Communications* **2017**, *8*, 15117. https://doi.org/10/f945q7.

FIGURES

Table 1: Comparison of fluorescence flow cytometry, spontaneous Raman flow cytometry, and coherent Raman flow cytometry.

	Information content	Quantitativeness	Throughput	Molecular specificity	Sensitivity	Interference with biological function	Inmunogenicity	Cytotoxicity	Cell sorting functionality
Fluorescence flow cytometry	up to 12	High	10,000 eps	Fluorescence	1 nM - 1 μM	Label dependent	Label dependent	Label dependent Photo dependent	Commercial
Spontaneous Raman flow cytometry	Multivariate	Calibration required	1 eps	Molecular vibrations	1 mM	None: Label free	None: Label free	Photo dependent	Low throughput
Coherent Raman flow cytometry	Multivariate	Calibration required	100 eps	Coherent molecular vibrations	1-10 mM	None: Label free	None: Label free	Photo dependent	Limited reports

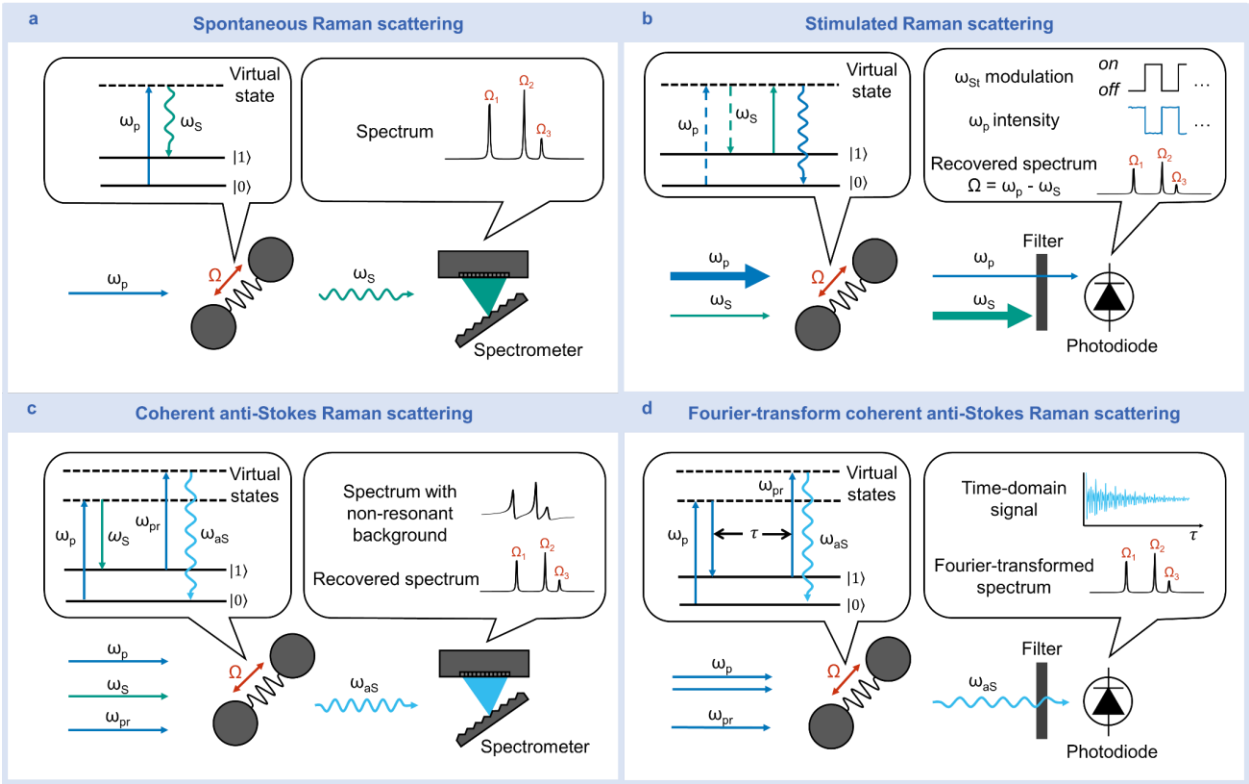

Figure 1: Energy and detection diagrams of spontaneous and coherent Raman scattering. (a) Spontaneous Raman scattering. (b) Stimulated Raman scattering. (c) Coherent anti-Stokes Raman scattering. (d) Fourier transform coherent anti-Stokes Raman scattering. Solid lines represent vibrational levels, dashed lines represent virtual levels, straight arrows represent incident photons, and squiggly arrows represent created photons. The SRS modulation scheme depicts stimulated Raman loss detection. Continuous and dashed arrows correspond to interactions of the electromagnetic fields with the ket and bra sides, respectively. Ω: molecular vibration frequency; ω_p: pump frequency; ω_S: Stokes frequency; ω_{pr}: probe frequency; ω_{aS}: anti-Stokes frequency.

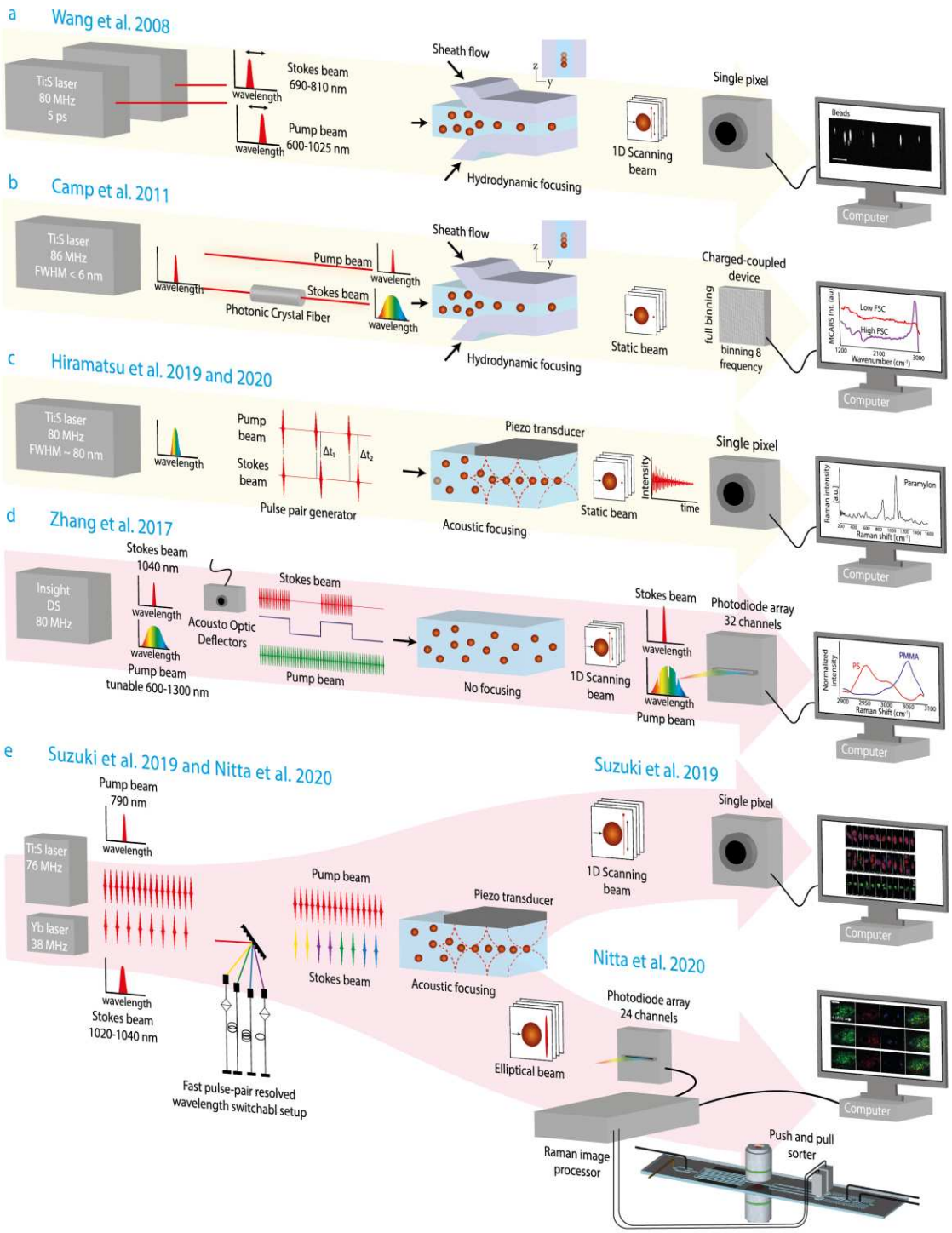

Figure 2: Schematics of the coherent Raman flow cytometers and sorters reported in the literature. (a) CARS flow cytometer adapted with permission from ref. 28. Copyright (2008) © The Optical Society. (b) CARS flow cytometer adapted with permission from ref. 30. Copyright (2011) © The Optical Society. (c) FT-CARS flow cytometer adapted with permission from ref. 2. Copyright (2020) © The Optical Society. (d) SRS flow cytometer adapted with permission from ref. 31. Copyright (2017) © The Optical Society. (e) SRS imaging flow cytometer and SRS image-activated cell sorter adapted with permission from ref. 3. CCBY-NC-ND (2019) PNAS and adapted with permission from ref. 4. CC BY 4.0 (2020) Nature, respectively.

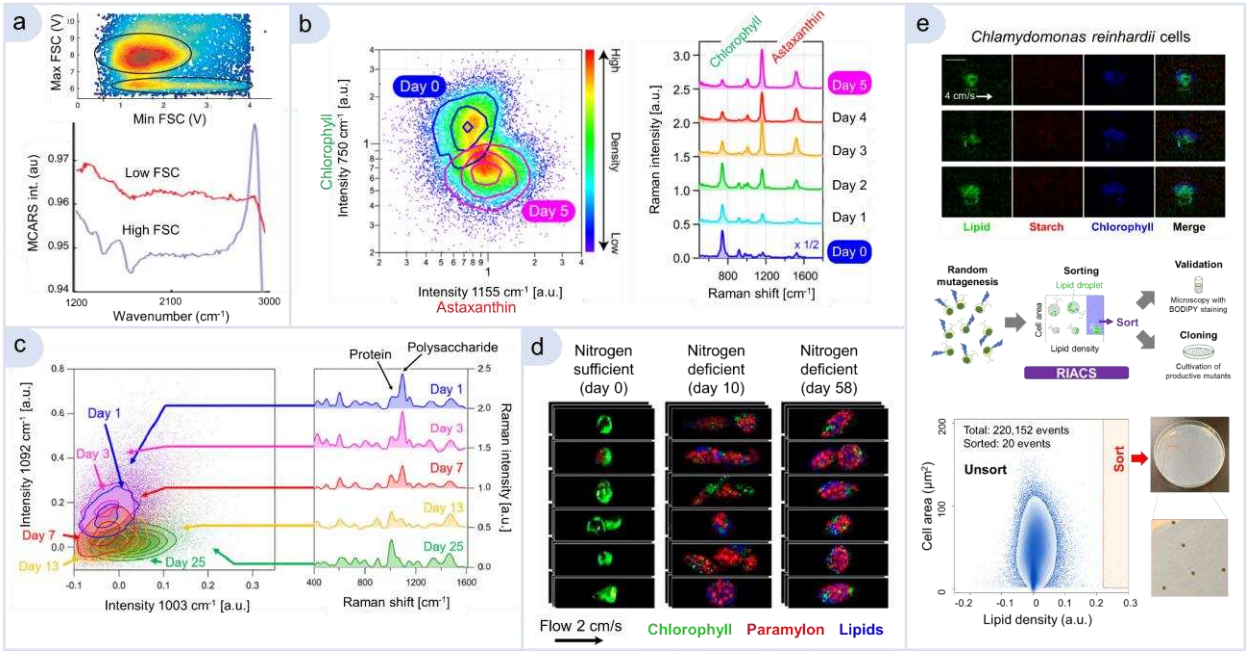

Figure 3: Coherent Raman flow cytometry of microbial cells. (a) Analysis of *S. cerevisiae* cells, adapted with permission from ref. 30. Copyright (2011) © The Optical Society. (b) Analysis of *H. lacustris* cells, adapted with permission from ref. 1. Copyright (2019) © The Optical Society. (c) Analysis of the paramylon content of *E. gracilis* cells, adapted with permission from ref. 2. Copyright (2020) Science. (d) Analysis of the spatial characteristics of *E. gracilis* cells, adapted with permission from ref. 3. Copyright (2019) the Authors. e) SRS image-activated sorting of lipid-rich *C. reinhardtii* cells, adapted with permission from ref. 4. Copyright (2020) Nature.

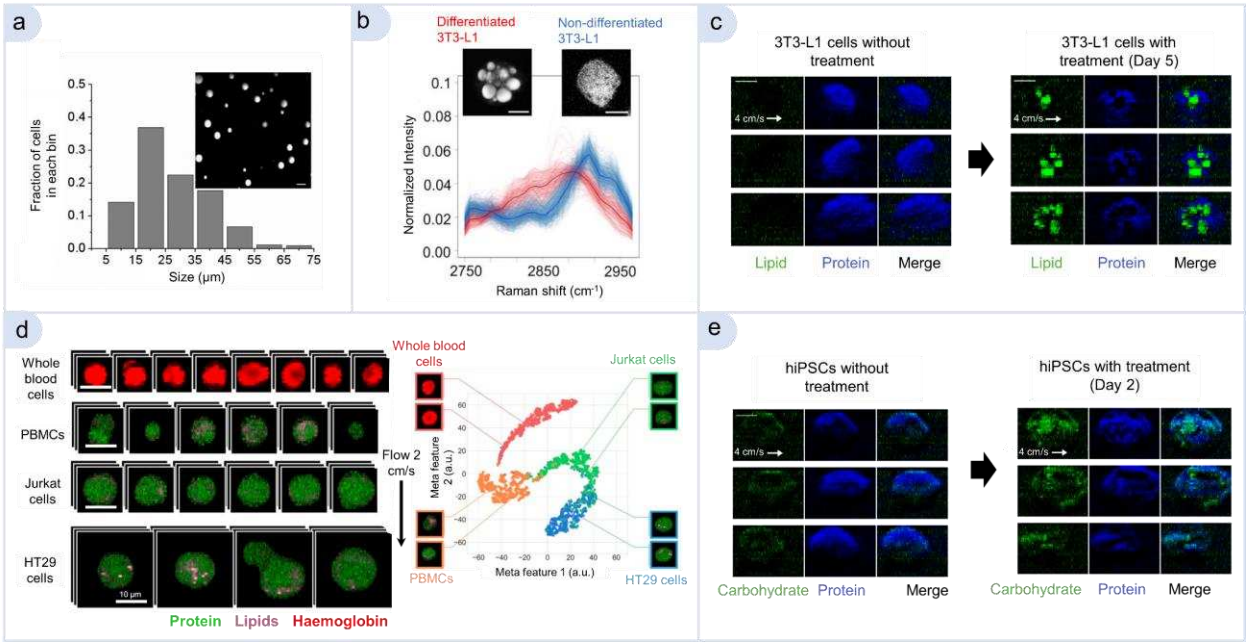

Figure 4: Coherent Raman flow cytometry of mammalian cells. (a) Analysis of mammary tissue mouse adipocytes, adapted with permission from ref. 28. Copyright (2008) © The Optical Society. (b) Analysis of differentiated 3T3-L1 murine adipocytes, adapted with permission from ref. 31. Copyright (2017) © The Optical Society. (c) SRS image-activated sorting of adipocyte-like cells, adapted with permission from ref. 4. Copyright (2020) Nature (d) Detection and classification of cancer cells in blood, adapted with permission from ref. 3. Copyright (2019) the Authors. (e) Analysis of hiPSCs in naïve and primed pluripotent states, adapted with permission from ref. 4. Copyright (2020) Nature.